13th International Symposium on Particle Image Velocimetry – ISPIV 2019
Munich, Germany, July 22-24, 2019

3D-LIF Experiments in an Open Wet Clutch by means of Defocusing PTV

Robin Leister[1*], **Jochen Kriegseis**[1]

[1] Karlsruhe Institute of Technology, Institute of Fluid Mechanics, 76131 Karlsruhe, Germany

[*] robin.leister@kit.edu

Abstract

Defocusing particle tracking velocimetry (DPTV) is applied to sub-millimetre rotor-stator gap flows on a test rig of an open wet clutch model. A recently proposed in-situ calibration approach (Fuchs et al., 2016) is modified to account for both the rotating no-slip condition and the grooves of the clutch lamella. Fluorescent particles are used to suppress the reflection issues at the walls and the groove patterns. The results demonstrate that DPTV is capable to derive sufficiently accurate velocity information in the smooth *Couette-like* gap region. Moreover, the experiments uncover formerly unknown flow properties inside the lamella grooves. The results provide evidence that the application of DPTV is a promising means to achieve a deeper insight into cause-effect relations between the flow fields inside an open wet clutch and the resulting adverse drag-torque characteristics.

1 Introduction

Fuel saving trends of automotive industry remain highly important due to a strict regulation of vehicle CO_2-emissions. Idling conditions of wet clutches present an essential research topic in this area, since undesired drag torque is generated due to strong shearing of the oil in open clutch state (Neupert et al., 2018). To date, a deeper understanding of the underlying mechanism(s) still requires more detailed knowledge of the flow in this gap, where still mostly integral torque measurements serve as basis for modelling and prediction efforts (see e.g. Jibin et al., 2012; Yang et al., 2012). Accordingly, existing clutch-flow models provide only limited and simplified (if at all) information on the velocity distributions. The reader is referred to Huang et al. (2012); Iqbal et al. (2013) and Pahlovy et al. (2016) for more details on recent clutch-flow models. In order to reduce the adverse drag torque, various lamella groove patterns have been identified; see e.g. Missimer and Johnson (1982); Razzaque and Kato (1999) or Takagi et al. (2011). However, the choice of the respective groove pattern mainly relies on experience, since the geometry modifications further increase the degree of complexity and cause-effect relations between the chosen pattern and the resulting drag torque remain yet to be fully understood. Some example groove patterns are illustrated in Figure 1(a).

Earlier investigations by Kriegseis et al. (2016) qualified a LDV profile sensors (LDV-PS) in combination with standard 2D2C PIV as candidating to determine velocity profiles in such sub-millimetre gap domains. In particular, the phase-locked measurements allowed a successful extraction of the groove-pattern foot print from the raw data. However, the limitations of the chosen 2D2C PIV configuration only provided mean velocity fields, which were averaged along the gap height. In continuation of these earlier efforts, the present work centers around the qualification of Defocusing Particle Tracking Velocimetry (DPTV) as a means to provide phase averaged 3D3C information in the gap of such rotor-stator configurations. Similar to the standard 2D2C setup, DPTV is a single camera flow measurement technique, which exists over two decades (see Raffel et al., 2018, for more details). Olsen and Adrian (2000) derived a theory, where the defocused particle image diameters are a hyperbola, which can be approximated as a linear function of the distance to the focal layer in a limited range, which in the present case is the gap height. Accordingly, an appropriately defocused 2D2C setup with moderate width of the light sheet might serve as a proper means for DPTV experiments.

An additional challenge for accurate DPTV measurements is the calibration issue in thin gaps, where it's difficult (if at all possible) to mount and unmount targets in the measurement domain without at least partly dissembling the test rig. To overcome such shortcomings an *in situ* calibrated approach for wall bounded

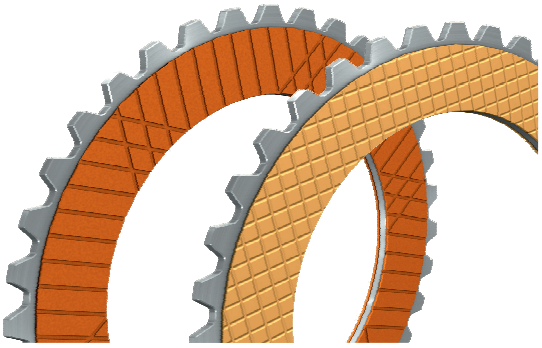

(a) Various lamella geometries as used in wet running clutches: ■ grouped parallel grooves and ■ waffle grooves (Source: www.ortlinghaus.com, copyright © 2019 Ortlinghaus-Werke GmbH, reprinted with permission)

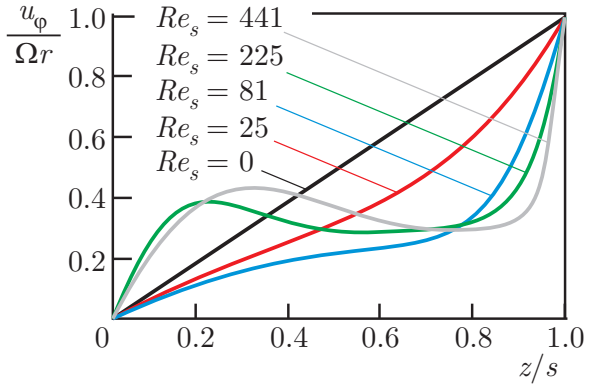

(b) Normalized gap profile of circumferential velocity (for various gap Reynolds numbers Re_s (adapted from Lance and Rogers, 1962).

Figure 1: Rotor-stator characteristics: (a) examples for grooved rotor surfaces, (b) disk-normal profiles of circumferential velocity u_φ for smooth rotor-stator systems and various gap Reynolds numbers Re_s.

measurements was introduced by Fuchs et al. (2016), which takes advantage of the zero-displacement at the solid (stationary) walls to retroactively identify the defocused particle image diameter for the depth position of the walls. This approach is applied in the present study of sub-millimetre gap flow, however, with modified boundary conditions to account for the angular speed of the no-slip condition at the clutch lamella; see Figure 1(b).

2 Experimental setup

To advance beyond the former proof-of-concept stage of Kriegseis et al. (2016), a new test rig has been developed, which rotates real clutch lamellae and provides optical access through a transparent stator (anti-reflection coated float-glass window); see Figure 2(a). Furthermore, the new rig allows an adjustable radial flow rate of oil, which provides a valuable additional degree of freedom in order to test realistic parameter conditions for future drag torque studies. Figure 2(b) shows the relevant geometry parameters of the test section. The inner surface of the glass plate spans a $r-\varphi$ - plane, which is chosen as origin of the perpendicularly oriented z-coordinate. A clutch lamella with radially oriented grooves ($h = 0.97$ mm; $w = 1.35$ mm) was chosen to adjust a gap height of $s = 0.6$ mm. The inner and outer radii of the lamella are $r_o = 93.75$ mm and $r_i = 82.5$ mm, respectively. Fluorescent particles ($d = 10.42$ μm, $\lambda_{em} = 584$ nm) are chosen due to significant amounts of reflection at the clutch walls and the lamella, which are illuminated with a Quantel Evergreen laser (70mJ/pulse). The focal plane is adjusted inside the lamella, so that the particle diameters increase with decreasing z-coordinate towards the glass plate, as also shown in Figure 2(b).

Two sets of experiments are performed for two fields of view (FOV) as indicated in Figure 3(a). The first set (Exp A) is conducted in the smooth part of the open wet clutch (FOV I) in order to testify the in-situ calibration for the rotating no-slip condition. Particularly, the boundary conditions at the glass plate and the rotating lamella are $u_\varphi(\varphi, r, z = 0) = 0$ and $u_\varphi(\varphi, r, z = s) = \Omega\, r$, respectively.

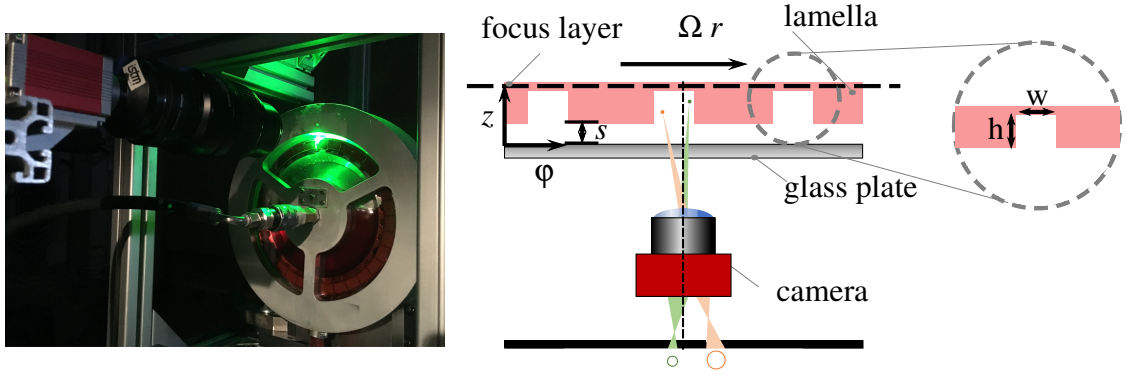

(a) Picture of the DPTV setup.

(b) Sketch of the measurement volume between stationary glass plate and rotating lamella; cartoon of defocused particles on the camera chip.

Figure 2: Experimental setup for the DPTV measurements; (a) picture of the test rig, optical access of laser through a top window in the clutch housing (b) sketch of the gap between rotating lamella and stationary glass plate with cartoon of two defocused particles and corresponding image diameters on the chip.

The defocussed particles are recorded with an ILA.PIV.Nano camera in double frame mode. The magnification factor is set to $M = 1.11$ with a corresponding reproduction scale of $5.77\ \mu\mathrm{m/px}$. Following the recommendations by Fuchs et al. (2016), a low source density of $n_{ppp} \approx 2 \cdot 10^{-4}$ particles per pixel has been chosen; see Table 1 for further experimental details. Figure 3(b) shows the center part of a random double frame raw image, where the frames are color-coded for clarity. A Hough-Transform (Hough, 1959) is applied to identify both diameter and center of the recorded circles. This procedure has sub-pixel accuracy, such that no pixel locking occurs due to the chosen processing strategy; see Figure 4(a). Approximately 150000 circles are identified, where $\approx 8\%$ ambiguous pairs or lost particles are ignored for the subsequent post-processing. Particle pairs are identified with a nearest neighbour algorithm inside a given estimation window. The FOV is divided into 25 px $\times$ 25 px sub-domains (SD), which are calibrated separately to account for lens imperfections and/or camera misalignment (cp. Fuchs et al., 2016). The gap-Reynolds number for the chosen parameter combinations is $Re_s = \Omega s^2/\nu \approx 10^{-2}$, which allow a straight *Couette-like* approximation for the circumferential velocity profile u_φ; cp. black line in Figure 1(b) and see Lance and Rogers (1962) for details.

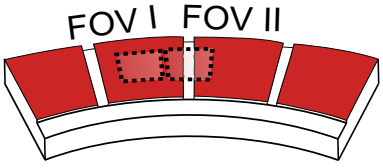

(a) Overview of the FOVs on the lamella.

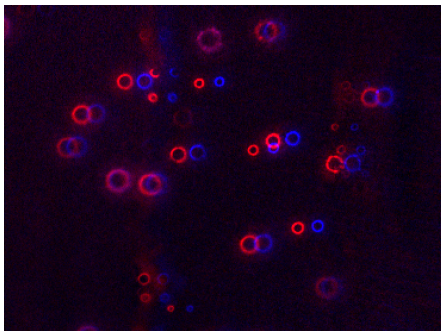

(b) Color coded raw image, red: frame 1; blue frame 2

Figure 3: (a) Different φ-positions of the FOV (b) color-coded raw image; note that the particle displacement increases for decreasing diameters.

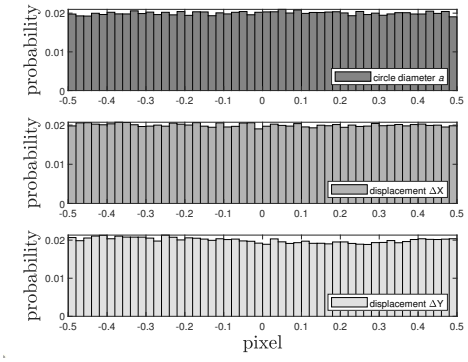

(a) subpixel distribution

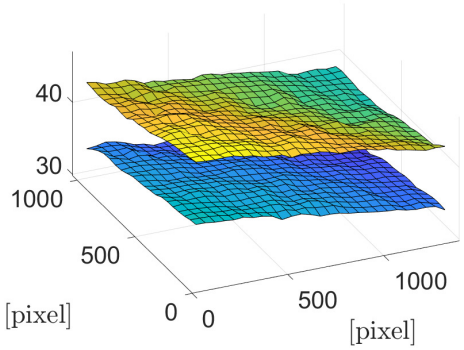

(b) Distribution of the diameters at the glass and the moving plate.

Figure 4: (a) Histogram of the circle diameter and displacements in x and y-direction (b) calibration of the physical coordinates, by means of local diameter detection of the fixed glass plate and the moving lamella.

The second set of experiments (Exp B) is conduced similar to Exp A, where only a distinctly different phase angle φ_g of the clutch lamella is chosen to record the radial groove in the center part of the image. The lamella boundary condition changes accordingly to $u_\varphi(\varphi_g, r, z = s+h) = \Omega\, r$ inside the groove. Similar to the findings of Kriegseis et al. (2016) a footprint of the groove is furthermore expected to become visible in the proximity of this cavity.

The defocussed particle images are recorded and processed similar to the above-outlined approach of Exp A. However, the unknown velocity profile inside the groove renders a robust estimation of the flow in the immediate cavity-bottom vicinity impossible, such that direct allocation of the no-slip condition is difficult. In order to avoid such calibration issues, a custom multi-step concept is applied.

First, the focal plane is set beyond the bottom of the groove so that the particle in the groove have a defocused diameter of a few pixels (FOV II). As a second step, the phase angle is changed to record 1500 frames in the smooth region (FOV I) at identical settings, which allows a calibration of the diameters for the glass and lamella locations analogue to Exp A for all SD inside the FOV (see Figure 4(b)). Then, the phase angle is reset to FOV II to record 1500 images above the groove, which is the main part of Exp B. Based on the assumption of a linear interrelation between z-location and defocused particle image diameter according to Fuchs et al. (2016), the particle locations inside the cavity are subsequently estimated by means of a diameter extrapolation up to the bottom of the cavity at $z = 1.57$ mm as the second calibration step.

Table 1: Conducted experiments with chosen parameter combinations.

	Exp A	Exp B
Objective lens	# 2.8	# 2.8
Objective	105 mm + 20 mm spacer	105 mm +20 mm spacer
Size FOV [mm]	6.00 × 8.03 mm^2	6.38 × 8.54 mm^2
FOV №	I	II
angular velocity Ω [1/s]	7.0	18.5
pulse distance Δt [μs]	150	80
number of images [mm]	800	1500

3 Results

Raw data and Couette fit are shown in Figure 5(a) for a SD in the center part of the raw images. Note that two abscissa and ordinate labels are provided to indicate the quantities before and after calibration. The calibrated velocity information is subsequently mapped onto a 3D grid to extract velocity maps of the gap flow. The circumferential gap velocity distribution in the $r-z$ plane is shown in 5(b). The measurements retroactively validate existing models of smooth rotor-stator configurations (see e.g. Iqbal et al., 2013)) and

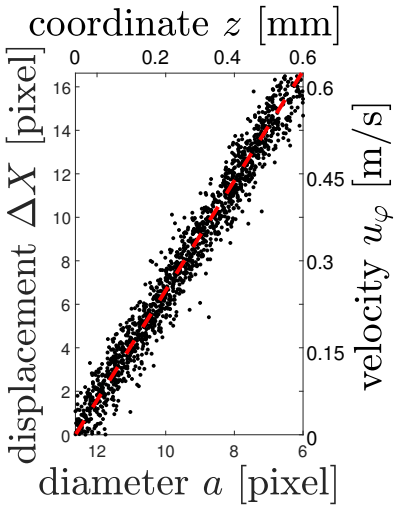

(a) Linear Couette profile for a SD in the FOV center

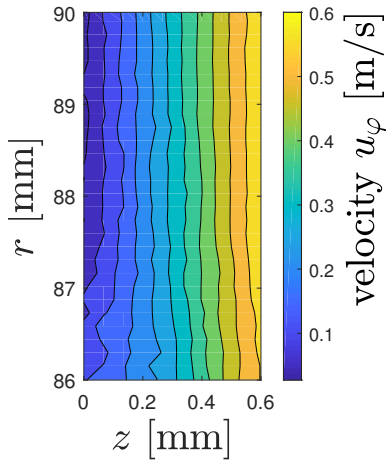

(b) Contour plot of u_φ across the gap

Figure 5: (a) determined velocity profile of a 0.3×0.3 mm^2 SD before and after calibration; (b) circumferential velocity u_φ in a $r-z$ plane.

show that the influence of the groove is negligible for a sufficiently large distance. The flow forms a linear Couette-like profile as earlier shown by Lance and Rogers (1962).

The accuracy limits in the r and φ-direction are comparable to a standard 2D2C-PTV approach with low source density. The limit in z direction, in contrast, is immediately influenced by the chosen aperture, which is a kind of scaling parameter for the linear depth approximation (Olsen and Adrian, 2000). Accordingly, the accuracy of the Hough-circle based depth allocation of the detected particles immediately relies on the chosen f-number. However, the results indicate sufficient accuracy for an estimation of the formerly hidden velocity information in the gap of open wet clutches.

The expected flow in and above the groove is sketched in Figure 6(a) for the lab-fixed frame of reference. The Ωr-no-slip condition no longer applies for the lamella surface as was shown for the smooth region in Figure 5(a), but moves to the bottom of the groove. Note that the fasted velocity is not the rotating wall and circumferential flow speeds higher than Ωr are expected above the bottom wall inside the groove. The origin of this profile shape becomes more obvious in the lamella fixed frame of reference, where the groove appears to resemble a typical cavity flow in a rotating reference frame; see Figure 6(b). Accordingly, a roller is expected to occur inside the cavity (indicated in dashed blue), which in turn locally adds to Ωr.

The experimental results for the three subdomains as indicated color-coded in Figure 6(a) are shown in Figure 7(a). Even though less obvious than indicated in the sketches of Figure 6, circumferential velocities of

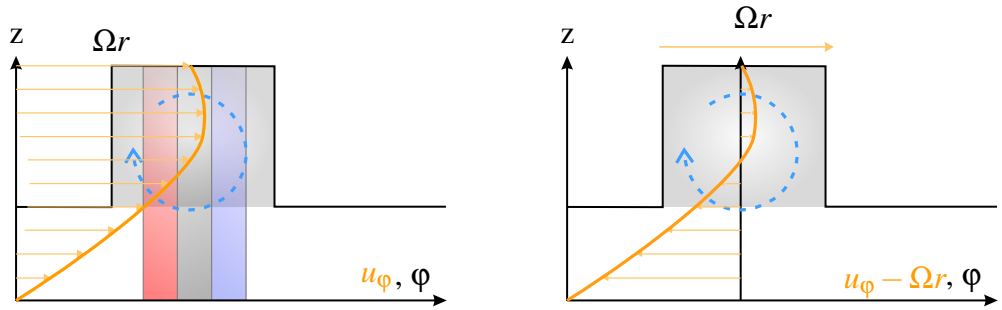

(a) lab-fixed reference system

(b) lamella-fixed reference frame

Figure 6: Sketch of the expected flow topology in the grooved lamella region.

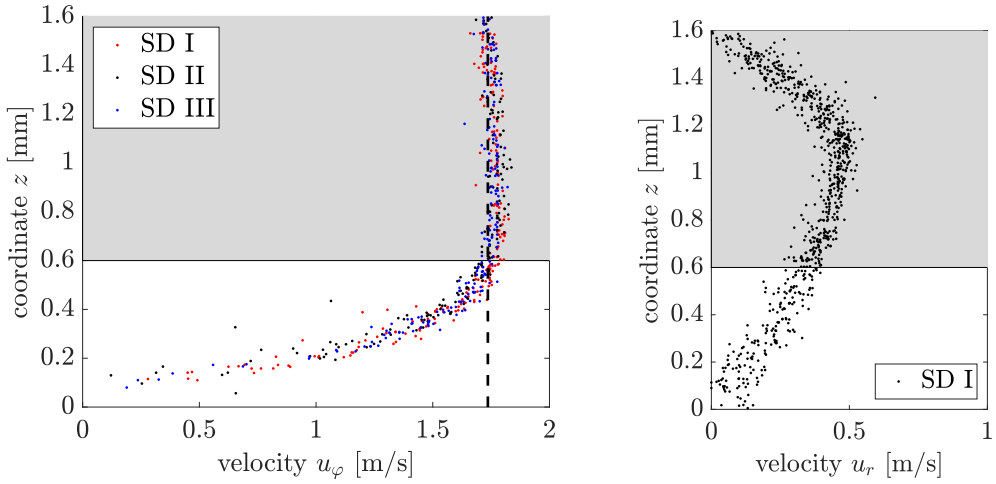

(a) velocity profile of the u_φ-component for three distinct sub-domains in the cavity

(b) velocity profile of the u_r-component in the middle of the cavity

Figure 7: Experimental results of (a) circumferential and (b) radial velocity components inside and above the grooved region.

$u_\varphi > \Omega r$ can be clearly identified inside the (gray shaded) cavity region, which demonstrates the occurrence of the expected roller-type flow pattern. Moreover, it is found that the Couette assumption in the region above the groove is still a good approximation. Interestingly enough, this is an important insight, since typical models treat the grooved region as non-existent for the drag torque calculation. This assumption is saliently uncovered to be an oversimplification of the underlying flow, as the remaining velocity gradient inevitably leads to a significant persistence of drag torque above the groove pattern. Furthermore, Figure 7(a) indicates an increased scatter margin for increased diameter of the defocused particle images.

Figure 7(b) additionally shows the radial velocity in the grooved region. The velocity above the groove is slightly shifted to the moving plate, due to centrifugal forces (cp. Leister et al., 2019). This finding is likewise important information as the radial volume fluxes are commonly considered be dominated by the fluxes in the non-grooved region.

4 Concluding remarks

The present work shows a proof-of-concept study, which aims at qualifying the method of defocusing particle (DPTV) image velocimetry for complex wall-bounded shear flows in sub-millimetre gaps of rotor-stator configurations. The in-situ calibration approach as proposed by Fuchs et al. (2016) has been adapted successfully to the present configuration of a rotating no-slip condition, where a multi-step approach takes care of groove patterns as complex boundary conditions. The results show a reasonable accuracy flow-topology characterization, which uncover formerly neglected shear-flow effects. In the ungrooved region with well defined boundary conditions the approach clearly confirms existing clutch-flow models. Moreover, for the grooved region the results reveal valuable and formerly hidden insights into the predominating flow patterns.

Two major conclusions can be drawn from the results. First, the DPTV approach demonstrates to be a promising complement to the LDV-PS method in so as to characterize and quantify the gap flow in open wet clutches. The 3D3C character of the DPTV leads to a clear identification of flow patterns, where a detailed LDV-PS based 1D2C analysis of axial velocity profiles across the clutch gap is hypothesized to allow a more precise of local shear magnitudes. Second, it must be concluded from the uncovered velocity information inside and in proximity of the groove indicates that typical clutch flow models still oversimplify the flow characteristics under consideration.

Finally, the results and drawn conclusions from the present feasibility study provide evidence that broader parameter studies of the considered flow scenario will provide an even deeper insight into the complex clutch flow phenomena as contributing to the adverse drag torque of open wet clutches.

References

Fuchs T, Hain R, and Kähler CJ (2016) In situ calibrated defocusing ptv for wall-bounded measurement volumes. *Measurement Science and Technology* 27:084005

Hough PVC (1959) Machine Analysis of Bubble Chamber Pictures. *Proceedings, 2nd International Conference on High-Energy Accelerators and Instrumentation, HEACC 1959: CERN, Geneva, Switzerland, September 14-19* C590914:554–558

Huang J, Wei J, and Qiu M (2012) Laminar flow in the gap between two rotating parallel frictional plates in hydro-viscous drive. *Chinese Journal of Mechanical Engineering* 25:144–152

Iqbal S, Al-Bender F, Pluymers B, and Desmet W (2013) Mathematical model and experimental evaluation of drag torque in disengaged wet clutches. *ISRN Tribology* 2013:1–16

Jibin H, Zengxiong P, and Chao W (2012) Experimental research on drag torque for single-plate wet clutch. *Journal of Tribology* 134:014502

Kriegseis J, Mattern P, and Dues M (2016) Combined planar piv and lda profile-sensor measurements in a rotor-stator disk configuration. *18th International Symposium on the Application of Laser and Imaging Techniques to Fluid Mechanics, Lisbon, Portugal, July 4-7,*

Lance GN and Rogers MH (1962) The axially symmetric flow of a viscous fluid between two infinite rotating disk. *Proceedings of the Royal Society of London Series A, Mathematical and Physical Sciences* 266:109–121

Leister R, Najafi AF, Kriegseis J, and Frohnapfel B (2019) Modelling concepts of open clutch flows - a theoretical approach. in *46th Leeds-Lyon Symposium on Tribology, Lyon, France*

Missimer JR and Johnson WS (1982) Flow between a smooth stationary disk and grooved rotating disk. *Journal of Lubrication Technology* 104:248–254

Neupert T, Benke E, and Bartel D (2018) Parameter study on the influence of a radial groove design on the drag torque of wet clutch discs in comparison with analytical models. *Tribology International* 119:809 – 821

Olsen MG and Adrian RJ (2000) Out-of-focus effects on particle image visibility and correlation in microscopic particle image velocimetry. *Experiments in Fluids* 29:S166–S174

Pahlovy SA, Mahmud SF, Kubota M, Ogawa M, and Takakura N (2016) Prediction of drag torque in a disengaged wet clutch of automatic transmission by analytical modeling. *Tribology Online* 11:121–129

Raffel M, Willert CE, Scarano F, Kähler CJ, and Wereley ST (2018) *Particle Image Velocimetry*. Springer-Verlag GmbH

Razzaque MM and Kato T (1999) Effects of groove orientation on hydrodynamic behavior of wet clutch coolant films. *Journal of Tribology* 121:56–61

Takagi Y, Nakata H, Okano Y, Miyagawa M, and Katayama N (2011) Effect of two-phase flow on drag torque in a wet clutch. *Journal of Advanced Research in Physics* 2:021108

Yang S, Wang H, and Guo F (2012) Experimental investigation on the groove effect in hydrodynamic lubrication. *Proceedings of the Institution of Mechanical Engineers, Part J: Journal of Engineering Tribology* 226:263–273